Materials Science and Engineering B 159–160 (2009) 202–205

Contents lists available at ScienceDirect

Materials Science and Engineering B

journal homepage: www.elsevier.com/locate/mseb

Study on the time decay of excess carriers in solar silicon

K. Lauer[a,b,*], A. Laades[a], H. Übensee[a], A. Lawerenz[a]

[a] CiS Institut für Mikrosensorik GmbH, SolarZentrum Erfurt, Konrad-Zuse-Str. 14, 99099 Erfurt, Germany
[b] TU Ilmenau, Institut für Physik, Weimarer Str. 32, 98693 Ilmenau, Germany

ARTICLE INFO

Article history:
Received 29 April 2008
Received in revised form
17 September 2008
Accepted 9 October 2008

Keywords:
Silicon
Photoconductivity

ABSTRACT

An understanding of the measured excess carrier decay in solar silicon is needed for a meaningful characterization of the material quality by this method. This paper studies the time decay of excess carriers after laser pulse excitation in solar silicon. For this material, which exhibits a high density of different defects, a simplified approach to solve the diffusion equation of the excess carriers can be taken. We calculate the time decay of the excess carriers numerically by using an appropriate model of the bulk minority carrier lifetime. These calculations are subsequently compared to experimental data, which are obtained by measuring the photoconductance decay using reflected microwaves in surface passivated solar silicon wafers. A very good agreement between theoretical and experimental results gives the base for further evaluation of interstitial iron and minority carrier traps using the excess carrier decay.

1. Introduction

At present the volume of solar silicon production exceeds the production of silicon for the semiconductor industry, since the photovoltaic market is rapidly growing. The differences between both types of material arise from the differing requirements in the respective industry sector. An extremely pure silicon is needed to fabricate microelectronic chips, whereas silicon used to produce solar cells has to be cheap, but still sufficiently pure for solar cells with high efficiency. The cost reduction is reached by decreasing the quality standards and by introducing simplified production processes. This leads to silicon, which contains a large amount of different defects and impurities. This type of silicon is referred to as solar silicon. Due to the robustness of the solar cell process, the solar silicon quality can be lower than the quality of silicon used in microelectronics. To clarify the question, which quality of solar silicon can produce efficient solar cells, appropriate characterization methods are needed.

A widely used tool to characterize the quality of silicon is the microwave detected photoconductance decay (MWPCD) system. This tool determines the time decay of the excess carriers after laser pulse excitation using the change in the reflectivity of the silicon, which is detected by reflected microwaves [1]. An exponential fit of these data reveals a time constant, which is interpreted as the effective minority carrier lifetime [2]. For thin and surface passivated solar silicon wafers an advanced evaluation method can be applied to MWPCD measurements, which allows to extract the bulk minority carrier lifetime as a function of the excess carrier density [3]. To get a deeper understanding of this evaluation method, this paper focuses on the comparison of the measured excess carrier decay with the respective numerical simulations. For this purpose we simplify the diffusion equation of the excess carriers assuming a spatial homogenous excess carrier profile during the decay. The remaining differential equation is solved numerically taking into account different Shockley–Read–Hall recombination processes and also Auger recombination. Comparable calculations are done for example by Ahrenkiel et al. [4].

2. Theory and simulation results

The density of the excess electrons $\Delta n(\vec{x}, t)$ in silicon is derived by solving the diffusion equation with proper initial and boundary conditions. For vanishing electrical field the diffusion equation in p-type silicon is [5]:

$$\frac{\partial \Delta n(\vec{x}, t)}{\partial t} = G - U + D\nabla^2 \Delta n(\vec{x}, t), \quad (1)$$

where G and U are the generation and the recombination rates, respectively. If we assume a homogenous carrier profile after turning off the laser ($G=0$) [3], this equation can be simplified by neglecting the third term on the right side. Taking into account different recombination processes like Auger [6] and

* Corresponding author at: CiS Institut für Mikrosensorik GmbH, SolarZentrum Erfurt, Konrad-Zuse-Str. 14, 99099 Erfurt, Germany. Tel.: +49 361 663 12 11; fax: +49 361 663 14 13.
E-mail address: klauer@cismst.de (K. Lauer).

0921-5107/$ – see front matter © 2008 Elsevier B.V. All rights reserved.
doi:10.1016/j.mseb.2008.10.009

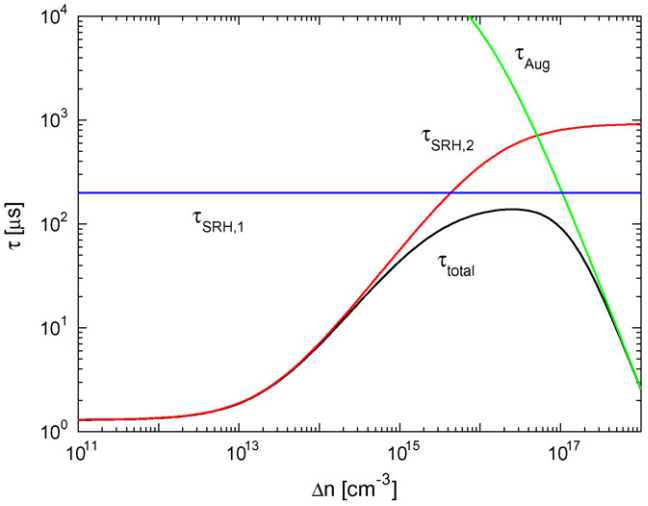

Fig. 1. Recombination lifetime as a function of the excess carrier density. The impact of three different recombination channels on the total lifetime is illustrated.

Shockley–Read–Hall (SRH) [7] recombination, the simplification yields

$$\frac{d\ \Delta n}{dt} = -\frac{\Delta n}{\tau_{\mathrm{Aug}}(\Delta n)} - \frac{\Delta n}{\tau_{\mathrm{SRH},1}} - \frac{\Delta n}{\tau_{\mathrm{SRH},2}(\Delta n)}. \quad (2)$$

This is a first order differential equation, which can be solved numerically. The influence of the different recombination channels on the total minority carrier lifetime τ_{total} is depicted in Fig. 1. The Auger coefficients are taken from Ref. [8]. For the first SRH recombination channel a constant lifetime of $\tau_{\mathrm{SRH},1} = 200\ \mu\mathrm{s}$ is assumed. The second SRH recombination lifetime is calculated for the interstitial iron defect [9] assuming a density of $[Fe_i] = 1.4 \times 10^{12}\ \mathrm{cm}^{-3}$ within a p-type sample ($p_0 = 1.6 \times 10^{16}\ \mathrm{cm}^{-3}$) at room temperature. These values apply to all figures displayed in this paper (except for Fig. 3). The total lifetime below an excess carrier density of $\Delta n = 10^{15}\ \mathrm{cm}^{-3}$ is dominated by the second SRH lifetime as is shown in Fig. 1. Above an excess carrier density of $\Delta n = 10^{17}\ \mathrm{cm}^{-3}$ Auger recombination determines the total lifetime. In between the first SRH lifetime mainly affects the total lifetime.

This lifetime characteristic is typical for solar silicon, because this material is usually contaminated with iron, which frequently dominates the lifetime. The impact of other defects is approximated by the second constant SRH recombination channel. Using this lifetime characteristic we solve Eq. (2) numerically [10]. Fig. 2 shows the results for different initial excess carrier densities $\Delta n(t=0) = \Delta n_0$. With ascending Δn_0 the signal moves upwards the τ_{total}-curve of Fig. 1. Above an initial excess carrier density of $\Delta n_0 = 10^{13}\ \mathrm{cm}^{-3}$ the effect of the increasing lifetime is clearly visible at the beginning of the simulated decay.

The impact of different interstitial iron contamination levels on the decay of the excess carriers is displayed in Fig. 3. Based on experimental data obtained in the next section, an initial condition of $\Delta n_0 = 2.3 \times 10^{15}\ \mathrm{cm}^{-3}$ is chosen. Fig. 3 clarifies the effect of different interstitial iron contents on the decay of the excess carriers and hence on the minority carrier lifetime. A slight change in the interstitial iron content leads to a large change in the excess carrier decay.

In p-type silicon interstitial iron forms meta-stable pairs with the acceptor, e.g. boron [11]. These pairs can easily be dissociated for example by illuminating the wafer at 1 sun for 1 min. Depending on the material this procedure is usually sufficient for a complete dissociation of the iron boron pairs [12]. Repairing takes place while storing the wafer in darkness for 24 h. It is a fully reversible process. To simulate the excess carrier decay during the dissociation process, a fourth recombination channel is added to Eq. (2), which accounts for the iron boron pair defect. The SRH parameters for this defect are taken from Ref. [13]. The numerical results for different interstitial iron to iron boron pair content ratios are plotted in Fig. 4.

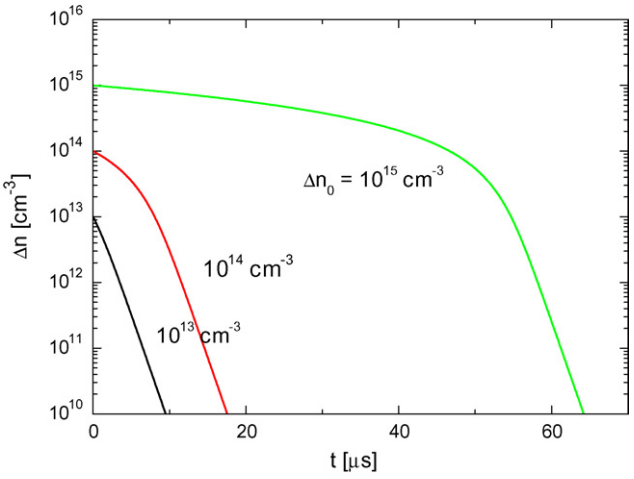

Fig. 2. Simulated time decay of the excess carriers for different initial excess carrier densities ($\Delta n_0 = 10^{13}$–$10^{15}\ \mathrm{cm}^{-3}$).

3. Experimental results

The solutions of Eq. (2) derived in the previous section are now to be compared to experimental data. For this purpose a typical solar silicon wafer (directionally solidified multicrystalline silicon) with a thickness of 200 µm and a high interstitial iron content is investigated. The surfaces are passivated by a silicon nitride layer, which ensures a low surface recombination velocity [14]. This is needed to guarantee a homogenous carrier profile during the most part of the measurement [3]. The time decay of the excess carriers is measured using a MWPCD (Semilab WT2000) device, which detects the change in the reflectivity after laser pulse excitation using reflected microwaves. This signal is, in the case of low injection condition ($\Delta n \ll p_0$), proportional to the excess carrier density [1]. The excess carriers are generated by a 200 ns laser pulse with a wavelength of 904 nm and an intensity of 16.4 W cm^{-2}. The spot size of the laser

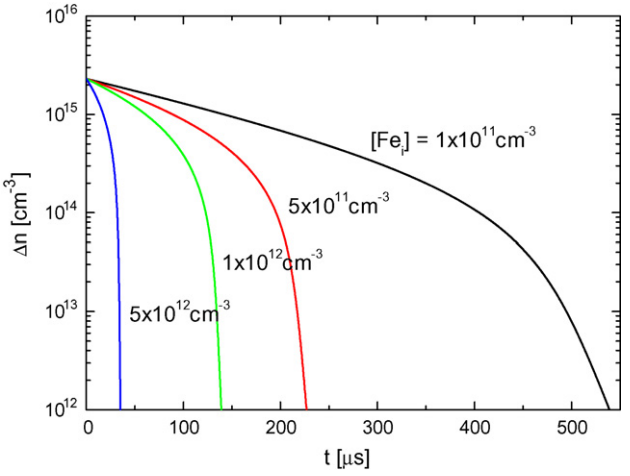

Fig. 3. Simulated time decay of the excess carriers for varying interstitial iron concentrations.

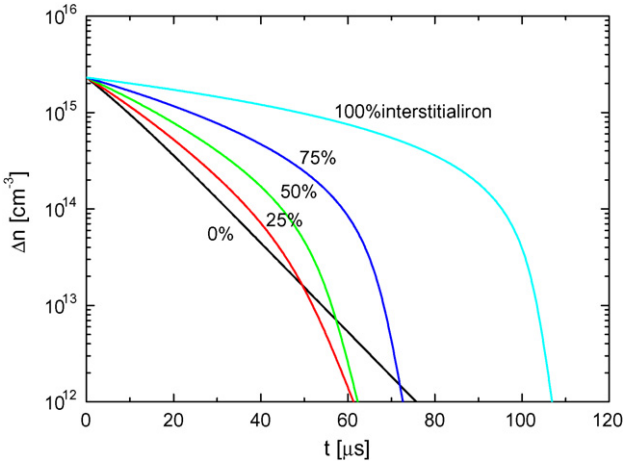

Fig. 4. Simulated time decay of the excess carriers during the dissociation of the iron boron pairs.

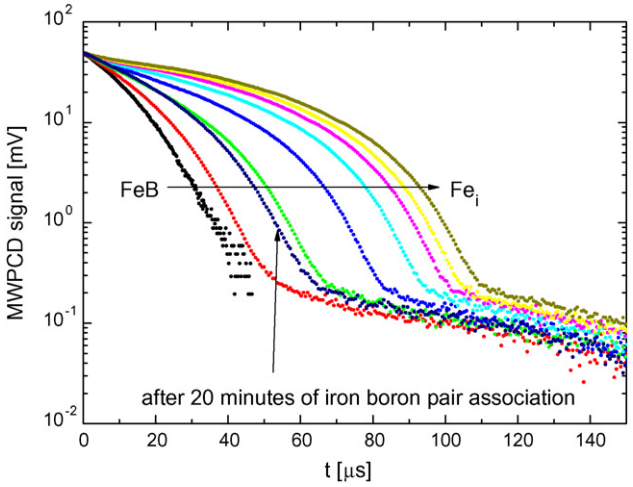

Fig. 6. Measured excess carrier decay during the dissociation of the iron boron pairs.

is about 1 mm^2. A four point probe tester is used to determine the doping density of the wafer to $p_0 = 1.6 \times 10^{16}$ cm^{-3}. The interstitial iron concentration of $[Fe_i] = 1.4 \times 10^{12}$ cm^{-3} is obtained by applying the method of Ref. [3].

Fig. 5 demonstrates the dependence of the measured excess carrier decay on the laser intensity. An increase of the intensity over two orders of magnitude results in an increase of MWPCD signal amplitude over nearly the same range. This confirms the proportionality between the measured signal and the excess carrier density. If these results of the measurement are compared to the simulation in Fig. 2, the excess carrier density level during the measurement can be identified to be in the mid to low injection level range. Also a large deviation at the tail of the excess carrier decay is observed. This can be explained by trapping of minority carriers [15].

The dissociation of the iron boron pairs has quite a pronounced effect on the measured excess carrier decay as can be seen in Fig. 6. Just like predicted by the simulation in Fig. 4 a large change in the signal is observed. The iron boron pairs are dissociated using the laser of the MWPCD measurement system. To avoid dissociation during the measurement of the excess carrier decay in the iron boron pair state, only the average of four measurements is taken. This leads to a noisy signal in the iron boron pair state (see Fig. 6).

The rest of the excess carrier decay curves are averaged over 1024 measurements. A complete dissociation of the iron boron pairs is reached after an illumination of about 10^5 pulses of the MWPCD measurement laser. If the illumination is turned off, the signal moves back to its initial state, as shown in Fig. 6. This proves the origin of the changing signal under illumination to be the iron boron pairs, because the regeneration at this time scale is characteristic only for these pairs.

In Fig. 7, the measured excess carrier decay of Fig. 6 is fitted by the numerical simulation in both states of the iron boron pairs. There are only two free parameters, which have to be adjusted for a simulation of the measured excess carrier decay. This is the initial excess carrier density and the constant SRH lifetime. The first one is more critical to the shape of the excess carrier decay than the second one. In fact this fitting routine can be used as a calibration of the MWPCD signal. If the determined initial value of the excess carrier density is compared to the doping density of the wafer, it is found that the low injection condition during the measurement is fulfilled. For the most part of the excess carrier decay, a very good agreement between the simulated and measured curve is observed. Only at the tail of the decay both curves deviate due to the impact of the trapping effect.

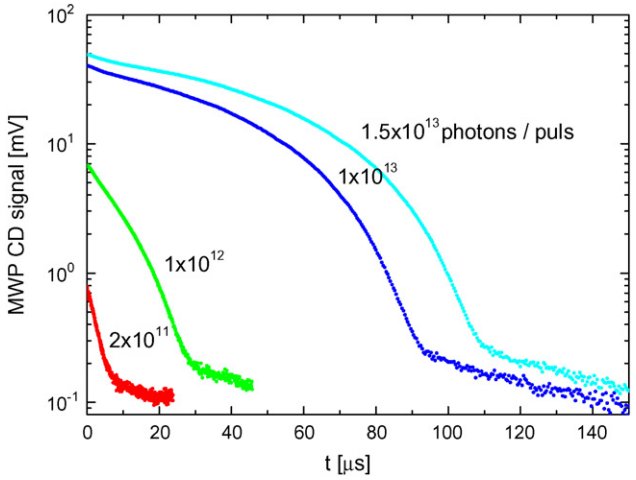

Fig. 5. Measured excess carrier decay for different intensities of the exciting laser.

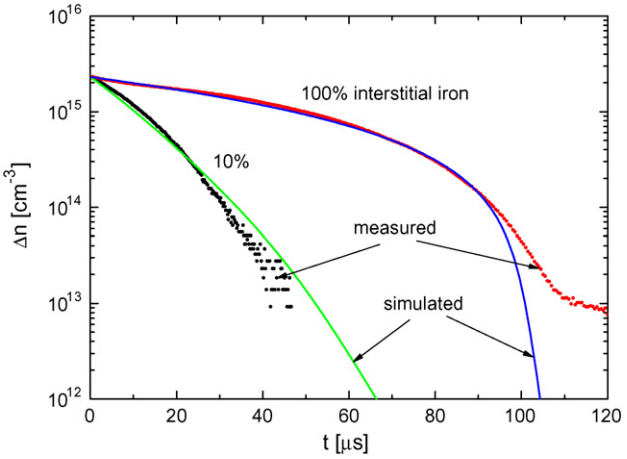

Fig. 7. Comparison of the measured and simulated excess carrier decay in both states of the iron boron pairs.

4. Conclusion

In this paper the diffusion equation of the excess carriers in solar silicon is numerically solved assuming a homogenous carrier profile and using an appropriate model for the minority carrier lifetime. The model includes three recombination channels: Auger recombination, a constant SRH recombination term and a SRH recombination term resulting from the interstitial iron defect. We simulated and measured the excess carrier decay for a variety of parameters and also during the dissociation process of the iron boron pairs. A very good agreement between the simulation and the measurement was found. Hence, the assumptions made for the simulations apply for passivated solar silicon wafers. The impact of an inhomogenous carrier profile during the measurement on the measured excess carrier density is negligible. Also the linearity between microwave signal and excess carrier density is approved to be a good approximation. Finally the minority carrier lifetime model, as applied for the simulations, is shown to be well suited for solar silicon. Based on these results an advanced evaluation method can now be applied to the excess carrier decay measured by microwave reflection in order to investigate interstitial iron, minority carrier traps or other defects in solar silicon.

Acknowledgement

The funding of this work by the State of Thuringia under project DEFIS (2006 WF 0100) is gratefully acknowledged.

References

[1] M. Kunst, G. Beck, J. Appl. Phys. 60 (1986) 3558.
[2] D.C. Gupta, W.M. Hughes, F.R. Bacher, Recombination Lifetime Measurements in Silicon, ASTM International, West Conshohocken, 1998.
[3] K. Lauer, A. Laades, H. Übensee, A. Lawerenz, H. Metzner, Proceedings of the 22nd European PVSEC, Milano, 2007, p. 1344.
[4] R.K. Ahrenkiel, B.M. Keyes, S. Johnston, Surf. Eng. 16 (2000) 54.
[5] S.M. Sze, Physics of Semiconductor Devices, 2nd edition, Wiley, New York, 1981, p. 51.
[6] A.R. Beatti, P.T. Landsberg, Proc. Royal Soc., A 429 (1958) 16.
[7] W. Shockley, W. Read, Phys. Rev. 87 (1952) 835.
[8] J. Dziewor, W. Schmid, Appl. Phys. Lett. 31 (1977) 346.
[9] A.A. Istratov, H. Hieslmair, E.R. Weber, Appl. Phys. A 69 (1999) 13.
[10] Wolfram Research, Inc., Mathematica, Version 4.0, Champaign, IL, 1999.
[11] K. Graff, H. Pieper, J. Electrochem. Soc. 128 (1981) 669.
[12] L.J. Geerligs, D. Macdonald, Appl. Phys. Lett. 85 (2004) 5227.
[13] D. Macdonald, A. Cuevas, J. Wong-Leung, J. Appl. Phys. 89 (2001) 7932.
[14] T. Lauinger, J. Schmidt, A.G. Aberle, R. Hezel, Appl. Phys. Lett. 68 (1996) 1232.
[15] D. Macdonald, A. Cuevas, Appl. Phys. Lett. 74 (1999) 1710.